

High-Performance HZO/InAlN/GaN MIS-HEMT with f_T/f_{\max} of 155/250 GHz

Peng Cui, Hang Chen, John Q. Xiao, and Yuping Zeng

Abstract—Scaling of GaN high-electron-mobility transistors (HEMTs) usually increases gate leakage current and deteriorates breakdown characteristic, limiting the maximum drain current and output power density. These bottlenecks can be circumvented by inserting a dielectric material under the gate of HEMTs. Doped HfO_2 is an excellent dielectric material but unexplored so far as the gate material of HEMTs for high-speed device application. Here we demonstrate that Zr-doped HfO_2 (HZO)-gated InAlN/GaN metal-insulator-semiconductor (MIS) HEMTs exhibit remarkable properties. The device with a gate length (L_g) of 50 nm exhibits maximum drain current ($I_{d,\max}$) of 2.15 A/mm, a transconductance (g_m) peak of 476 mS/mm, an on/off current ratio (I_{on}/I_{off}) of 9.3×10^7 , a low drain-induced barrier lowering (DIBL) of 45 mV/V. RF characterizations reveal a current gain cutoff frequency (f_T) of 155 GHz and a maximum oscillation frequency (f_{\max}) of 250 GHz, resulting in a $(f_T \times f_{\max})^{1/2}$ of 197 GHz. The breakdown voltages (BV) of 35 V and 72 V is achieved on the $L_g = 50$ nm devices with source-drain distance (L_{sd}) of 0.6 and 2 μm (f_T of 155 and 110 GHz), resulting in high Johnson’s figure-of-merit ($\text{JFOM} = f_T \times \text{BV}$) of 5.4 and 7.9 THz·V, respectively. These properties, particularly the high f_T/f_{\max} and JFOM are highly desirable for the millimeter-wave power applications, demonstrating the great technological potential of HZO/InAlN/GaN MIS-HEMTs.

Index Terms— $\text{Hf}_{0.5}\text{Zr}_{0.5}\text{O}_2$; GaN MIS-HEMT; f_T/f_{\max} ; breakdown voltage; JFOM.

I. INTRODUCTION

GaN-based high-electron-mobility transistors (HEMTs) indicate great potential for RF and millimeter-wave power applications [1-5]. To date, excellent current gain cutoff frequency (f_T) and maximum oscillation frequency (f_{\max}) have been demonstrated on GaN HEMTs with device scaling [6-9]. However, device scaling usually causes high gate leakage current and deteriorates breakdown voltage (BV), thus limiting the maximum drain current and output power density. The gate dielectric can suppress the leakage current and enhance the breakdown characteristic. Therefore, the introduction of gate dielectric on GaN metal-insulator-semiconductor HEMTs (MIS-HEMTs) could lead to further improvement of the device performance for high-speed and high-power applications.

For high-speed device application, different dielectric materials (Al_2O_3 [10-19], HfO_2 [20-22], SiN [23-27], SiO_2 [28], TiO_2 [29], MgCaO [30], ZnO [31], *et al.*) have been investigated as the gate dielectric in GaN MIS-HEMTs. The relevant device performance, such as maximum drain current ($I_{d,\max}$) of 2.4 A/mm [32], on/off current ratio (I_{on}/I_{off}) of 5×10^8

[30], transconductance (g_m) of 653 mS/mm [11], f_T/f_{\max} of 190/300 GHz [20], and Johnson’s figure-of-merit (JFOM) of 10.8 THz·V [23] has been demonstrated. Although there is still a gap between MIS-HEMTs and HEMTs, the advantages of MIS-HEMTs have been shown.

In this study, we report the first demonstration of the $\text{Hf}_{0.5}\text{Zr}_{0.5}\text{O}_2$ (HZO) as the gate dielectric for GaN-based high-speed MIS-HEMTs. Key device performance parameters, including high $I_{d,\max}$, low drain-induced barrier lowering (DIBL), high f_T/f_{\max} and JFOM, are simultaneously achieved on the HZO/InAlN/GaN MIS-HEMTs, suggesting their great potential for high-speed applications.

II. EXPERIMENT

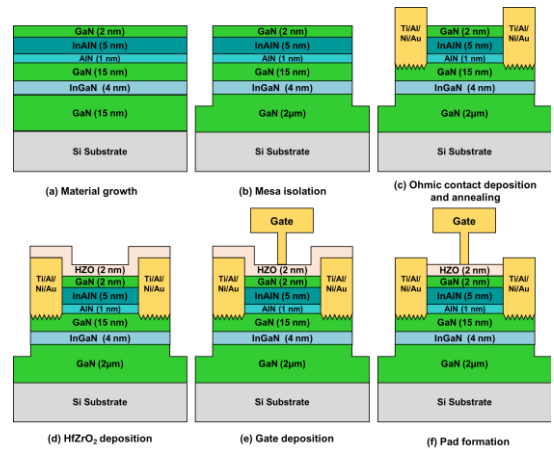


Fig. 1. Key process flow for the fabricated HZO/InAlN/GaN HEMT: (a) material growth, (b) mesa isolation, (c) ohmic contact deposition and annealing, (d) HZO gate dielectric deposition, (e) gate deposition, and (f) pad formation.

Fig. 1 shows the key process flow of the fabricated HZO/InAlN/GaN MIS-HEMT. The growth of epitaxial structures is performed with metalorganic chemical vapor deposition (MOCVD) on a 4-inch high-resistance Si substrate. The epitaxial layer consists of a 2- μm undoped GaN buffer layer, a 4-nm $\text{In}_{0.12}\text{Ga}_{0.88}\text{N}$ back-barrier layer, a 15-nm GaN channel layer, a 1-nm AlN interlayer, a 5-nm lattice-matched $\text{In}_{0.17}\text{Al}_{0.83}\text{N}$ barrier layer, and a 2-nm GaN cap layer. Device mesa isolation was carried out with Cl_2 -based inductively coupled plasma (ICP) etching with an etch depth of ~ 300 nm. Then ohmic contact was formed with Ti/Al/Ni/Au deposition and annealing at 850 °C for 40 s. Then HZO was deposited as the gate dielectric and passivation layer by using plasma-enhanced atomic layer deposition (PEALD) at 150 °C.

This work was supported in part by the NASA International Space Station under Grant 80NSSC20M0142, and in part by Air Force Office of Scientific Research under Grant FA9550-19-1-0297 and Grant FA9550-21-1-0076.

P. Cui and Y. Zeng are with the Department of Electrical and Computer Engineering, University of Delaware, Newark, DE, 19716, USA (e-mail: yzeng@udel.edu).

H. Chen and J. Q. Xiao are with the Department of Physics and Astronomy, University of Delaware, Newark, DE 19716, USA.

Tetrakis(dimethylamino)hafnium (TDMAH), Bis(methyl- η^5 -cyclopentadienyl)methoxymethylzirconium (ZRCMMM), and oxygen are used as Hf, Zr, and O source, respectively. The film was grown in a Hf: Zr ratio of 1:1 by alternating cycles of TDMAH, O₂, ZRCMMM, O₂. The alternating cycles were repeated 30 times for 2-nm HZO growth. These steps were followed by T-shaped gate fabrication with electron beam lithography and Ni/Au deposition. Finally, HZO on the pad was removed by dipping the samples in HF solution (HF: H₂O = 1: 9) for 30s. Devices with source-drain distance (L_{sd}) of 2 ~ 0.6 μm , gate length (L_g) of 50 ~ 150 nm, and gate width (W_g) of $20 \times 2 \mu\text{m}$ were fabricated.

III. RESULTS AND DISCUSSION

Hall measurements were carried out on the InAlN/GaN heterostructure before and after HZO deposition. Before HZO deposition, the electron density (n_{2d}) of $1.71 \times 10^{13} \text{ cm}^{-2}$ and electron mobility (μ_{2d}) of $1663 \text{ cm}^2/\text{V}\cdot\text{s}$ are obtained, an indication of a good InAlN/GaN heterostructure. After HZO deposition, n_{2d} of $2.24 \times 10^{13} \text{ cm}^{-2}$ and μ_{2d} of $1613 \text{ cm}^2/\text{V}\cdot\text{s}$ are determined. The increased n_{2d} presents a good passivation effect on the material surface [33, 34], and the negligible change in μ_{2d} means that the electron mobility is not degraded with the dielectric deposition. **Fig. 2(a)** depicts the diode curves, which show a ~ 4 order decrease of gate leakage current at a gate-source voltage (V_{gs}) of -10 V with HZO deposition. **Fig. 2(b)** presents the extracted interface trap density (D_{it}) of the HZO/InAlN/GaN diode by using the conventional conductance method [35, 36]. The inset of **Fig. 2(b)** plots the measured and fitted G_p/ω versus ω (G_p is the measured conductance and ω is the radial frequency [35, 36]). The device shows a low D_{it} of $1\text{--}3 \times 10^{12} \text{ eV}^{-1}\cdot\text{cm}^{-2}$. The Fat-FET (HZO/InAlN/GaN with L_g of 96 μm and L_{sd} of 100 μm) is fabricated for low-field mobility extraction [37, 38]. **Fig. 2(c)** shows the measured capacitance and n_{2d} at a 1 MHz frequency of the Fat-FET. **Fig. 2(d)** exhibits low-field mobility (at $V_{ds} = 0.1 \text{ V}$) versus n_{2d} of the Fat-FET, indicating a peak mobility of $1627 \text{ cm}^2/\text{V}\cdot\text{s}$. All these properties unequivocally demonstrate that HZO a strong candidate as a gate dielectric for GaN MIS-HEMTs.

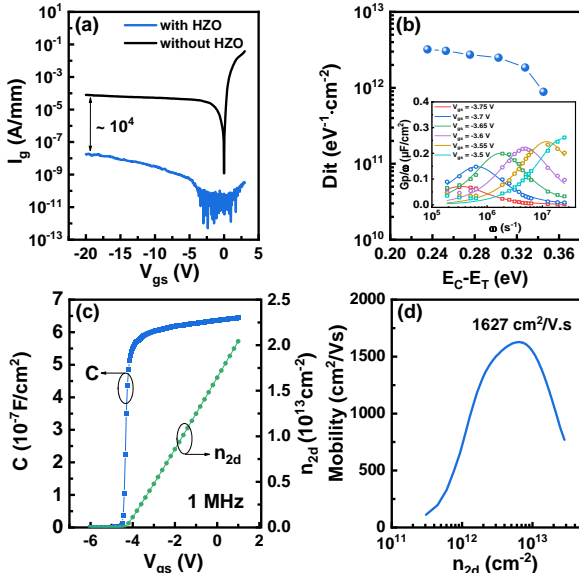


Fig. 2(a) I_g - V_{gs} curves for the InAlN/GaN and HZO/InAlN/GaN diode. **(b)** Extracted D_{it} as a function of E_C-E_T . Inset: Measured and fitted G_p/ω versus ω .

(c) Capacitance (C , left) and electron density (n_{2d} , right) versus V_{gs} . **(d)** Extracted low-field mobility versus n_{2d} with a peak value of $1627 \text{ cm}^2/\text{V}\cdot\text{s}$ on an HZO/InAlN/GaN MIS-HEMT with $L_g = 96 \mu\text{m}$ and $L_{sd} = 100 \mu\text{m}$.

Fig. 3(a) shows the typical output characteristic of the HZO/InAlN/GaN MIS-HEMT ($L_g = 50 \text{ nm}$, and $L_{sd} = 0.6 \mu\text{m}$), depicting an on-resistance (R_{on}) of $1.41 \Omega\cdot\text{mm}$. The transfer characteristic and transconductance (g_m) of the same device are shown in **Fig. 3(b)**. A maximum drain current ($I_{d,max}$) of 2.15 A/mm and a g_m peak of 476 mS/mm are observed. The transfer and gate current characteristics in semi-log scale at $V_{ds} = 10 \text{ V}$ and 1 V (**Fig. 3(c)**) exhibit a low leakage current, an on/off current ratio (I_{on}/I_{off}) of 9.3×10^7 , a subthreshold swing (SS) of 130 mV/dec, and a drain-induced barrier lowering (DIBL) of 45 mV/V at $I_d = 10 \text{ mA/mm}$. With gate dielectric deposition, the low DIBL confirms insignificant short-channel effects (SCEs) with an aspect ratio of ~5 [1, 39]. **Fig. 3(d)** shows the off-state three-terminal breakdown characteristics of the $L_g = 50 \text{ nm}$ HZO/InAlN/GaN MIS-HEMTs. The breakdown voltage (BV) of 72 V and 35 V is demonstrated on the device with L_{sd} of 2 and 0.6 μm , respectively.

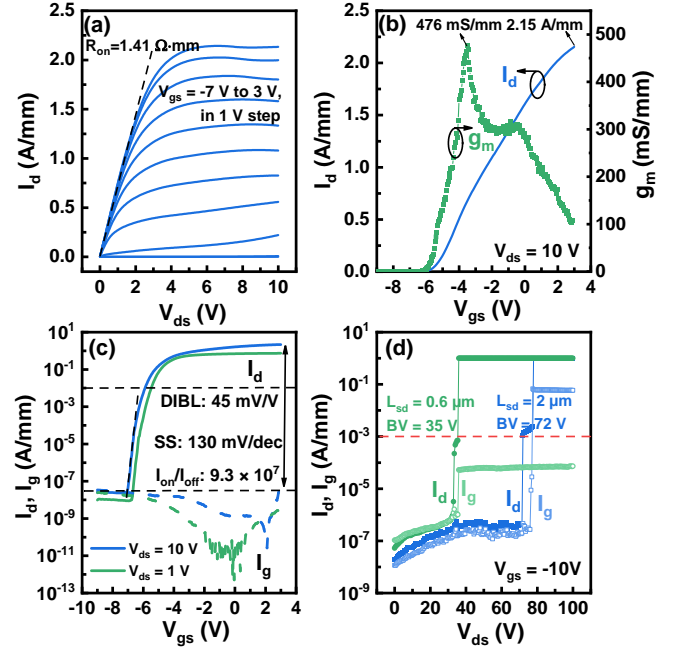


Fig. 3 (a) Output characteristic, **(b)** transfer characteristic in linear scale (left), transconductance (g_m , right), and **(c)** transfer and gate current characteristics in semi-log scale at V_{ds} of 10 V and 1 V of the $L_g = 50 \text{ nm}$ HZO/InAlN/GaN MIS-HEMT. **(d)** Off-state three-terminal breakdown characteristics for the $L_g = 50 \text{ nm}$ HZO/InAlN/GaN MIS-HEMTs with L_{sd} of 2 and 0.6 μm , respectively.

The microwave characteristics of the HZO/InAlN/GaN MIS-HEMTs are characterized from 1 to 65 GHz using an Anritsu MS4647B vector network analyzer. By using the de-embedded S-parameters, the high-frequency gains of the devices are extracted. **Fig. 4(a)** plots the measured short-circuit current gain ($|h_{21}|^2$), Mason's unilateral gain (U), maximum-stable-gain (MSG), and stability-factor (k) of the MIS-HEMT with L_g of 50 nm and L_{sd} of 0.6 μm at $V_{ds} = 10 \text{ V}$ and $V_{gs} = -3.8 \text{ V}$. f_T/f_{max} of 155/250 GHz is obtained by extrapolation of $|h_{21}|^2$ and U with a -20 dB/dec slope, resulting in $f_T \times L_g$ of $7.75 \text{ GHz}\cdot\mu\text{m}$ and $(f_T \times f_{max})^{1/2}$ of 197 GHz. f_T/f_{max} versus I_d is also measured and plotted in **Fig. 4(b)**. The classical 16-element equivalent-circuit model is used for the device, as shown in **Fig. 4(c)** [40, 41]. Based on the model, the device extrinsic and intrinsic parameters are extracted in **Fig. 4(d)** and the simulated $f_{T,model}$

$f_{\max, \text{model}}$ of 156/249 GHz are consistent with the measured results [40-42]. **Fig. 4 (e) and (f)** show the measured f_T/f_{\max} as a function of L_g and L_{sd} , respectively. f_T for the $L_g = 50$ nm devices with L_{sd} of 2 and 0.6 μm is 110 and 155 GHz (BV of 72 V and 35 V), resulting in the high Johnson's figure-of-merit (JFOM = $f_T \times \text{BV}$) of 7.9 and 5.4 THz-V, respectively. **Fig. 5(a) and (b)** show the f_{\max} and BV versus f_T benchmark for the presented devices against state-of-the-art GaN MIS-HEMTs on SiC, Sapphire, Si, and GaN substrates [10-32]. The HZO/InAlN/GaN MIS-HEMTs on Si in this work exhibit excellent device performance on high f_T/f_{\max} and BV simultaneously, indicating the outstanding potential for high-speed and high power applications.

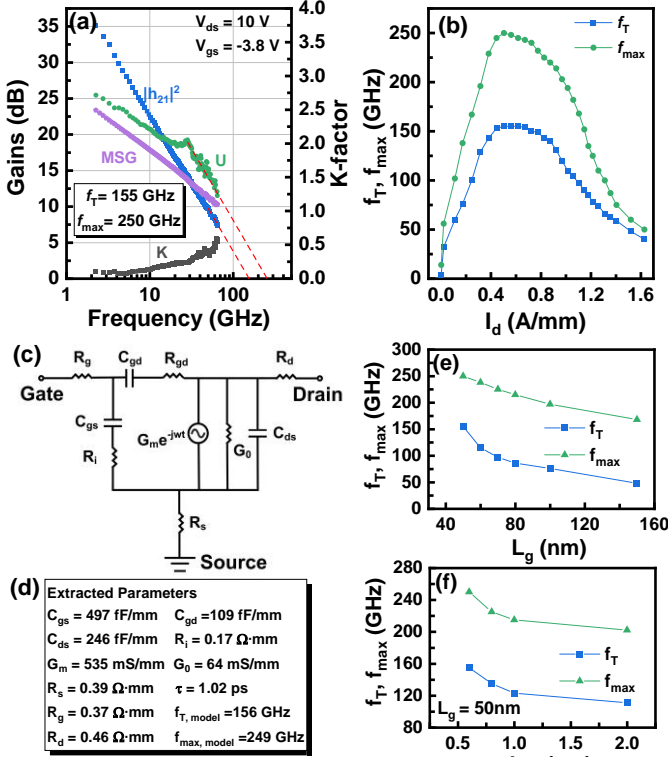


Fig. 4 (a) High-frequency gains ($|h_{21}|^2$, U and MSG), stability factor (k), **(b)** f_T/f_{\max} versus I_d , **(c)** small-signal equivalent-circuit model; and **(d)** the extracted intrinsic parameters of the $L_g = 50$ nm HZO/InAlN/GaN MIS-HEMT. **(e)** and **(f)** f_T/f_{\max} of HZO/InAlN/GaN MIS-HEMT as a function of L_g and L_{sd} , respectively.

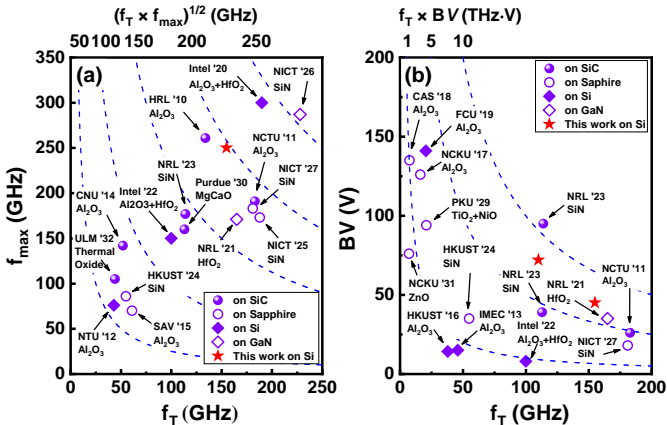


Fig. 5 (a) f_{\max} and **(b)** BV versus f_T benchmark for the presented devices (HZO/InAlN/GaN MIS-HEMTs on Si) against state-of-the-art GaN MIS-HEMTs on SiC, Sapphire, Si, and GaN substrates.

IV. CONCLUSION

In summary, by using HZO as the gate dielectric, the $L_g = 50$ nm InAlN/GaN MIS-HEMT presents a high performance with $I_{\text{ds, max}}$ of 2.15 A/mm, g_m peak of 476 mS/mm, $I_{\text{on}}/I_{\text{off}}$ of 9.3×10^7 , DIBL of 45 mV/V, f_T/f_{\max} of 155/250 GHz, and $(f_T \times f_{\max})^{1/2}$ of 197 GHz. The devices with L_{sd} of 2 and 0.6 μm present high JFOM of 7.9 and 5.4 THz-V, respectively. The simultaneously achieved excellent cutoff frequencies and breakdown characteristics indicate the great potential of the HZO/InAlN/GaN MIS-HEMTs for RF and millimeter wave power applications.

REFERENCES

- [1] K. Shinohara, D. C. Regan, Y. Tang, A. L. Corrión, D. F. Brown, J. C. Wong, J. F. Robinson, H. H. Fung, A. Schmitz, and T. C. Oh, "Scaling of GaN HEMTs and Schottky diodes for submillimeter-wave MMIC applications," *IEEE Trans. Electron Devices*, vol. 60, pp. 2982-2996, 2013, doi:10.1109/IEDM.2013.2268160.
- [2] M. Micovic, D. Brown, D. Regan, J. Wong, Y. Tang, F. Herrault, D. Santos, S. Burnham, J. Tai, and E. Prophet, "High frequency GaN HEMTs for RF MMIC applications," in *2016 IEEE International Electron Devices Meeting (IEDM)*, 2016, pp. 3.3. 1-3.3. 4, doi:10.1109/IEDM.2016.7838337.
- [3] Y.-K. Lin, S. Noda, H.-C. Lo, S.-C. Liu, C.-H. Wu, Y.-Y. Wong, Q. H. Luc, P.-C. Chang, H.-T. Hsu, and S. Samukawa, "AlGaIn/GaN HEMTs with damage-free neutral beam etched gate recess for high-performance millimeter-wave applications," *IEEE Electron Device Lett.*, vol. 37, pp. 1395-1398, 2016, doi:10.1109/LED.2016.2609938.
- [4] D. Marti, S. Tirelli, A. R. Alt, J. Roberts, and C. R. Bolognesi, "150-GHz Cutoff Frequencies and 2-W/mm Output Power at 40 GHz in a Millimeter-Wave AlGaIn/GaN HEMT Technology on Silicon," *IEEE Electron Device Lett.*, vol. 33, pp. 1372-1374, Oct. 2012, doi:10.1109/Led.2012.2204855.
- [5] R. C. Fitch, D. E. Walker, A. J. Green, S. E. Tetlak, J. K. Gillespie, R. D. Gilbert, K. A. Sutherlin, W. D. Gouty, J. P. Theimer, and G. D. Via, "Implementation of High-Power-Density X-Band AlGaIn/GaN High Electron Mobility Transistors in a Millimeter-Wave Monolithic Microwave Integrated Circuit Process," *IEEE Electron Device Lett.*, vol. 36, pp. 1004-1007, 2015, doi:10.1109/LED.2015.2474265.
- [6] Y. Tang, K. Shinohara, D. Regan, A. Corrión, D. Brown, J. Wong, A. Schmitz, H. Fung, S. Kim, and M. Micovic, "Ultrahigh-Speed GaN High-Electron-Mobility Transistors With f_T/f_{\max} of 454/444 GHz," *IEEE Electron Device Lett.*, vol. 36, pp. 549-551, 2015, doi:10.1109/LED.2015.2421311.
- [7] M. L. Schuette, A. Ketterson, B. Song, E. Beam, T.-M. Chou, M. Pilla, H.-Q. Tserng, X. Gao, S. Guo, and P. J. Fay, "Gate-recessed integrated E/D GaN HEMT technology with $f_T/f_{\max} > 300$ GHz," *IEEE Electron Device Lett.*, vol. 34, pp. 741-743, 2013, doi:10.1109/LED.2013.2257657.
- [8] J. W. Chung, T.-W. Kim, and T. Palacios, "Advanced gate technologies for state-of-the-art f_T in AlGaIn/GaN HEMTs," in *2010 International Electron Devices Meeting*, 2010, pp. 30.2. 1-30.2. 4, doi:10.1109/IEDM.2010.5703449.
- [9] L. Li, K. Nomoto, M. Pan, W. Li, A. Hickman, J. Miller, K. Lee, Z. Hu, S. J. Bader, and S. M. Lee, "GaN HEMTs on Si With Regrown Contacts and Cutoff/Maximum Oscillation Frequencies of 250/204 GHz," *IEEE Electron Device Lett.*, vol. 41, pp. 689-692, 2020, doi:10.1109/LED.2020.2984727.
- [10] A. Corrión, K. Shinohara, D. Regan, I. Milosavljevic, P. Hashimoto, P. Willadsen, A. Schmitz, S. Kim, C. Butler, and D. Brown, "High-Speed AlN/GaN MOS-HFETs With Scaled ALD Al_2O_3 Gate Insulators," *IEEE Electron Device Lett.*, vol. 32, pp. 1062-1064, 2011, doi:10.1109/LED.2011.2155616.
- [11] Y.-K. Lin, S. Noda, C.-C. Huang, H.-C. Lo, C.-H. Wu, Q. H. Luc, P.-C. Chang, H.-T. Hsu, S. Samukawa, and E. Y. Chang, "High-performance GaN MOSHEMTs fabricated with ALD Al_2O_3 dielectric and NBE gate recess technology for high frequency power applications," *IEEE Electron Device Lett.*, vol. 38, pp. 771-774, 2017, doi:10.1109/LED.2017.2696569.
- [12] Z. H. Liu, G. I. Ng, S. Arulkumaran, Y. K. T. Maung, K. L. Teo, S. C. Foo, V. Sahnuganathan, T. Xu, and C. H. Lee, "High Microwave-Noise Performance of AlGaIn/GaN MISHEMTs on Silicon With Al_2O_3 Gate

- Insulator Grown by ALD," *IEEE Electron Device Lett.*, vol. 31, pp. 96-98, 2009, doi:10.1109/LED.2009.2036135.
- [13] U. Peralagu, A. Alian, V. Putcha, A. Khaled, R. Rodriguez, A. Sibaja-Hernandez, S. Chang, E. Simoen, S. Zhao, and B. De Jaeger, "CMOS-compatible GaN-based devices on 200mm-Si for RF applications: Integration and Performance," in *2019 IEEE International Electron Devices Meeting (IEDM)*, 2019, pp. 17.2. 1-17.2. 4, doi:10.1109/IEDM19573.2019.8993582.
- [14] S.-I. Kim, H.-K. Ahn, J.-W. Lim, and K. Lee, "GaN MIS-HEMT PA MMICs for 5G Mobile Devices," *Journal of the Korean Physical Society*, vol. 74, pp. 196-200, 2019, doi:doi.org/10.3938/jkps.74.196.
- [15] P. Kordos, M. Mikulics, A. Fox, D. Gregusova, K. Cico, J.-F. Carlin, N. Grandjean, J. Novak, and K. Frohlich, "RF Performance of InAlN/GaN HFETs and MOSHFETs With $f_T \times L_g$ up to 21 GHz μm ," *IEEE Electron Device Lett.*, vol. 31, pp. 180-182, 2010, doi:10.1109/LED.2009.2038078.
- [16] T. Huang, J. Ma, X. Lu, Z. J. Liu, X. Zhu, and K. M. Lau, "Self - aligned gate - last enhancement - and depletion - mode AlN/GaN MOSHEMTs on Si," *physica status solidi (c)*, vol. 11, pp. 890-893, 2014, doi:doi.org/10.1002/pssc.201300493.
- [17] H.-Y. Liu, B.-Y. Chou, W.-C. Hsu, C.-S. Lee, J.-K. Sheu, and C.-S. Ho, "Enhanced AlGaIn/GaN MOS-HEMT performance by using hydrogen peroxide oxidation technique," *IEEE Trans. Electron Devices*, vol. 60, pp. 213-220, 2012, doi:10.1109/TED.2012.2227325.
- [18] S. Huang, X. Liu, J. Zhang, K. Wei, G. Liu, X. Wang, Y. Zheng, H. Liu, Z. Jin, and C. Zhao, "High RF performance enhancement-mode Al₂O₃/AlGaIn/GaN MIS-HEMTs fabricated with high-temperature gate-recess technique," *IEEE Electron Device Lett.*, vol. 36, pp. 754-756, 2015, doi:10.1109/LED.2015.2445353.
- [19] H.-Y. Liu, W.-C. Ou, and W.-C. Hsu, "Investigation of post oxidation annealing effect on H₂O₂-Grown-Al₂O₃/AlGaIn/GaN MOSHEMTs," *IEEE Journal of the Electron Devices Society*, vol. 4, pp. 358-364, 2016, doi:10.1109/JEDS.2016.2594293.
- [20] H. W. Then, S. Dasgupta, M. Radosavljevic, P. Agababov, I. Ban, R. Bristol, M. Chandhok, S. Chouksey, B. Holybee, and C. Huang, "3D heterogeneous integration of high performance high-K metal gate GaN NMOS and Si PMOS transistors on 300mm high-resistivity Si substrate for energy-efficient and compact power delivery, RF (5G and beyond) and SoC applications," in *2019 IEEE International Electron Devices Meeting (IEDM)*, 2019, pp. 17.3. 1-17.3. 4, doi:10.1109/IEDM19573.2019.8993583.
- [21] D. J. Meyer, D. A. Deen, D. F. Storm, M. G. Ancona, D. S. Katzer, R. Bass, J. A. Roussos, B. P. Downey, S. C. Binari, and T. Gougousi, "High electron velocity submicrometer AlN/GaN MOS-HEMTs on freestanding GaN substrates," *IEEE Electron Device Lett.*, vol. 34, pp. 199-201, 2013, doi:10.1109/LED.2012.2228463.
- [22] H. Then, L. Chow, S. Dasgupta, S. Gardner, M. Radosavljevic, V. Rao, S. Sung, G. Yang, and R. Chau, "High-performance low-leakage enhancement-mode high-K dielectric GaN MOSHEMTs for energy-efficient, compact voltage regulators and RF power amplifiers for low-power mobile SoCs," in *2015 Symposium on VLSI Technology (VLSI Technology)*, 2015, pp. T202-T203, doi:10.1109/VLSIT.2015.7223674.
- [23] B. P. Downey, D. J. Meyer, D. S. Katzer, J. A. Roussos, M. Pan, and X. Gao, "SiNx/InAlN/AlN/GaN MIS-HEMTs With 10.8 THz-V Johnson Figure of Merit," *IEEE Electron Device Lett.*, vol. 35, pp. 527-529, 2014, doi:10.1109/LED.2014.2313023.
- [24] X. Lu, J. Ma, H. Jiang, C. Liu, P. Xu, and K. M. Lau, "Fabrication and characterization of gate-last self-aligned AlN/GaN MISHEMTs with in situ SiNx gate dielectric," *IEEE Trans. Electron Devices*, vol. 62, pp. 1862-1869, 2015, doi:10.1109/TED.2015.2421031.
- [25] Y. Yamashita, I. Watanabe, A. Endoh, N. Hirose, T. Mimura, and T. Matsui, "Effect of source-drain spacing on DC and RF characteristics of 45 nm-gate AlGaIn/GaN MIS-HEMTs," *Electron. Lett.*, vol. 47, pp. 211-212, 2011, doi:10.1049/el.2010.3213.
- [26] I. Watanabe, Y. Yamashita, and A. Kasamatsu, "Research and Development of GaN-based HEMTs for Millimeter-and Terahertz-Wave Wireless Communications," in *2020 IEEE International Symposium on Radio-Frequency Integration Technology (RFIT)*, 2020, pp. 19-21, doi:10.1109/RFIT49453.2020.9226221.
- [27] M. Higashiwaki, T. Mimura, and T. Matsui, "30-nm-gate AlGaIn/GaN heterostructure field-effect transistors with a current-gain cutoff frequency of 181 GHz," *Jpn. J. Appl. Phys.*, vol. 45, p. L1111, 2006, doi:https://doi.org/10.1143/JJAP.45.L1111.
- [28] J. Bernat, D. Gregušová, G. Heidelberger, A. Fox, M. Marso, H. Lüth, and P. Kordoš, "SiO₂/AlGaIn/GaN MOSHFET with 0.7 μm gate-length and f_{max}/f_T of 40/24 GHz," *Electron. Lett.*, vol. 41, pp. 667-668, 2005, doi:10.1049/el:20050556.
- [29] D. Meng, S. Lin, C. P. Wen, M. Wang, J. Wang, Y. Hao, Y. Zhang, K. M. Lau, and W. Wu, "Low leakage current and high-cutoff frequency AlGaIn/GaN MOSHEMT using submicrometer-footprint thermal oxidized TiO₂/NiO as gate dielectric," *IEEE Electron Device Lett.*, vol. 34, pp. 738-740, 2013, doi:10.1109/LED.2013.2256102.
- [30] H. Zhou, X. Lou, K. Sutherlin, J. Summers, S. B. Kim, K. D. Chabak, R. G. Gordon, and D. Y. Peide, "DC and RF performance of AlGaIn/GaN/SiC MOSHEMTs with deep sub-micron T-gates and atomic layer epitaxy MgCaO as gate dielectric," *IEEE Electron Device Lett.*, vol. 38, pp. 1409-1412, 2017, doi:10.1109/LED.2017.2746338.
- [31] C.-T. Lee, Y.-L. Chiou, and C.-S. Lee, "AlGaIn/GaN MOS-HEMTs with gate ZnO dielectric layer," *IEEE Electron Device Lett.*, vol. 31, pp. 1220-1223, 2010, doi:10.1109/LED.2010.2066543.
- [32] M. Alomari, F. Medjdoub, J.-F. Carlin, E. Feltin, N. Grandjean, A. Chuvilín, U. Kaiser, C. Gaquière, and E. Kohn, "InAlN/GaN MOSHEMT with self-aligned thermally generated oxide recess," *IEEE Electron Device Lett.*, vol. 30, pp. 1131-1133, 2009, doi:10.1109/LED.2009.2031659.
- [33] Z. Liu, G. Ng, S. Arulkumaran, Y. Maung, K. Teo, S. Foo, and V. Sahmuganathan, "Improved two-dimensional electron gas transport characteristics in AlGaIn/GaN metal-insulator-semiconductor high electron mobility transistor with atomic layer-deposited Al₂O₃ as gate insulator," *Appl. Phys. Lett.*, vol. 95, p. 223501, 2009, doi:https://doi.org/10.1063/1.3268474.
- [34] Z. Liu, G. Ng, S. Arulkumaran, Y. Maung, K. Teo, S. Foo, and V. Sahmuganathan, "Improved Linearity for Low-Noise Applications in 0.25- μm GaN MISHEMTs Using ALD Al₂O₃ as Gate Dielectric," *IEEE Electron Device Lett.*, vol. 31, pp. 803-805, 2010, doi:10.1109/LED.2010.2051136.
- [35] P. Kordoš, R. Stoklas, D. Gregušová, and J. Novák, "Characterization of AlGaIn/GaN metal-oxide-semiconductor field-effect transistors by frequency dependent conductance analysis," *Appl. Phys. Lett.*, vol. 94, p. 223512, 2009, doi:doi.org/10.1063/1.3148830.
- [36] G. Ye, H. Wang, S. Arulkumaran, G. I. Ng, R. Hofstetter, Y. Li, M. Anand, K. Ang, Y. Maung, and S. C. Foo, "Atomic layer deposition of ZrO₂ as gate dielectrics for AlGaIn/GaN metal-insulator-semiconductor high electron mobility transistors on silicon," *Appl. Phys. Lett.*, vol. 103, p. 142109, 2013, doi:doi.org/10.1063/1.4824445.
- [37] O. Katz, A. Horn, G. Bahir, and J. Salzman, "Electron mobility in an AlGaIn/GaN two-dimensional electron gas. I. Carrier concentration dependent mobility," *IEEE Trans. Electron Devices*, vol. 50, pp. 2002-2008, 2003, doi:10.1109/TED.2003.816103.
- [38] N. Chowdhury, J. Lemettinen, Q. Xie, Y. Zhang, N. S. Rajput, P. Xiang, K. Cheng, S. Suihkonen, H. W. Then, and T. Palacios, "P-channel GaN transistor based on p-GaN/AlGaIn/GaN on Si," *IEEE Electron Device Lett.*, vol. 40, pp. 1036-1039, 2019, doi:10.1109/LED.2019.2916253.
- [39] G. H. Jessen, R. C. Fitch, J. K. Gillespie, G. Via, A. Crespo, D. Langley, D. J. Denninghoff, M. Trejo, and E. R. Heller, "Short-channel effect limitations on high-frequency operation of AlGaIn/GaN HEMTs for T-Gate devices," *IEEE Trans. Electron Devices*, vol. 54, pp. 2589-2597, Oct. 2007, doi:10.1109/Ted.2007.904476.
- [40] S. Bouzid-Driad, H. Maher, N. Defrance, V. Hoel, J.-C. De Jaeger, M. Renvoise, and P. Frijlink, "AlGaIn/GaN HEMTs on Silicon Substrate With 206-GHz f_{max} ," *IEEE Electron Device Lett.*, vol. 34, pp. 36-38, Jan. 2012, doi:10.1109/LED.2012.2224313.
- [41] G. Crupi, D. Xiao, D.-P. Schreurs, E. Limiti, A. Caddemi, W. De Raedt, and M. Germain, "Accurate multiband equivalent-circuit extraction for GaN HEMTs," *IEEE Trans. Microwave Theory Tech.*, vol. 54, pp. 3616-3622, 2006, doi:10.1109/TMTT.2006.882403.
- [42] C. F. Campbell and S. A. Brown, "An analytic method to determine GaAs FET parasitic inductances and drain resistance under active bias conditions," *IEEE Trans. Microwave Theory Tech.*, vol. 49, pp. 1241-1247, 2001, doi:10.1109/22.932242.